Optimization of Transient Behavior of Complex Turbocompressor Shaft Lines

Pieder Jörg
Member, IEEE
ABB Medium Voltage Drives
Austrasse
5300 Turgi, Switzerland
pieder.joerg@ch.abb.com

Andrea Lenzi
Electrical and Control Department
GE Oil & Gas
Via Felice Matteucci 2
50127 Firenze, Italy
andrea.lenzi@ge.com

Valerio Depau
Senior Diagnostics Engineer
GE Oil & Gas
Via Felice Matteucci 2
50127 Firenze, Italy
valerio.depau@ge.com

***Abstract* – A considerable number of papers appeared over the last two decades discussing the origin of torque ripple for the different variable speed drive technologies. Direct reaction of mechanical loads to this excitation was investigated deeply. However only recently, it was recognized that the drives and the mechanical shaft line form a closed-loop control system, and that – as they are interacting with each other both ways – the resulting torsional behavior may be quite different from the traditional considerations in feed forward from drive to shaft line. This paper shows how closed loop effects can take place, leading to momentary, unexpected high alternating torque, which could impact the shaft line integrity. It then focuses on the optimization of transient behavior in order to avoid potentially adverse interactions between converter control system and train dynamics.**

***Index Terms* – Turbomachinery, variable speed drives, electromechanical systems, closed loop systems, mechanical variables control, torque vibrations, damping.**

I. Introduction

The implementation of Variable Speed Drive Systems (VSDS) in oil & gas applications is relatively recent and it is rapidly proliferating in terms of number of units and installed power, passing in a few years from single line-up configurations (<10 MW) to very complex multi-thread high power systems (>25 MW). Such growth has posed new challenges in terms of electro-mechanical interaction and power quality requirements, stretching the development of VSDS to existing technology limits in terms of motor speed as well as output power.

Over the last two decades, VSDS of different technology were intensively discussed as sources of torque ripple and the direct reaction of mechanical loads to this excitation was investigated deeply. However only recently, it was recognized that the VSDS and the mechanical shaft line must also be interpreted as a closed-loop control system, and that – as they are interacting with each other both ways – the resulting torsional behavior may be quite different from the traditional considerations in open loop (feed forward from VSDS to shaft line). This is fundamental and applicable to all VSDS technologies and adds a new and very important aspect to the selection of the optimal VSDS technology for a specific project. While for complex turbocompressor shaft lines, like LNG trains, it is of capital importance to select properly the VSDS for highest reliability, thus reducing any risk of forced outage as much as possible; it is even more important to do a thorough electro-mechanical system integration of driver and load, in order to "bring home" the benefits of a VSDS, once the technology selection has been made.

Closed loop effects are typically characterized by rotor oscillations of the electric motor producing back electro-motive force oscillations, which result in disturbances to the electric power circuit of the inverter. Depending on the selected control strategy inside the VSDS, the inverter will react to these disturbances, again impacting the rotor behavior. It is obvious, that with an inadequate control strategy, this may result in a self sustaining limit cycle in the overall electro-mechanical system. It has to be noticed, that this closed loop effect can be developed irrespective of direct excitation of the mechanical resonance. Its final result is the superposition of a negative damping on the VSDS side to the positive mechanical damping of the train, reducing the overall damping and increasing the coupled electro-mechanical sensitivity even to very small air gap torque ripple (much less than 0.5% of inverter delivered torque).

The present study, performed on a large commercial installation, shows how closed loop effects can occur and lead to momentary, unexpected high alternating torque, which could impact the shaft line integrity (coupling fretting, fatigue, etc). It then focuses on the optimization of transient behavior (mainly at start up) in order to avoid potentially adverse interactions between converter control system and train dynamics.

II. System Description

A. *Compressor Train Description*

The study object for transient behavior optimization is composed by an 86MW gas turbine (GT), one axial compressor (CC1), one centrifugal compressor (CC2) and one 20MW electric helper motor (EM), fed by a dual channel (each channel 6-pulse) 22MVA LCI drive. An overview of this compressor train for production of liquefied natural gas (LNG) is shown in Fig. 1. C1 designates the GT drive end side coupling, C2 the coupling between CC1 and CC2 and C3 the EM drive end side coupling.

DOI: 10.1109/IAS.2011.6074307

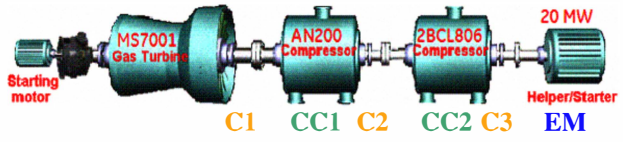

Fig. 1. LNG train overview

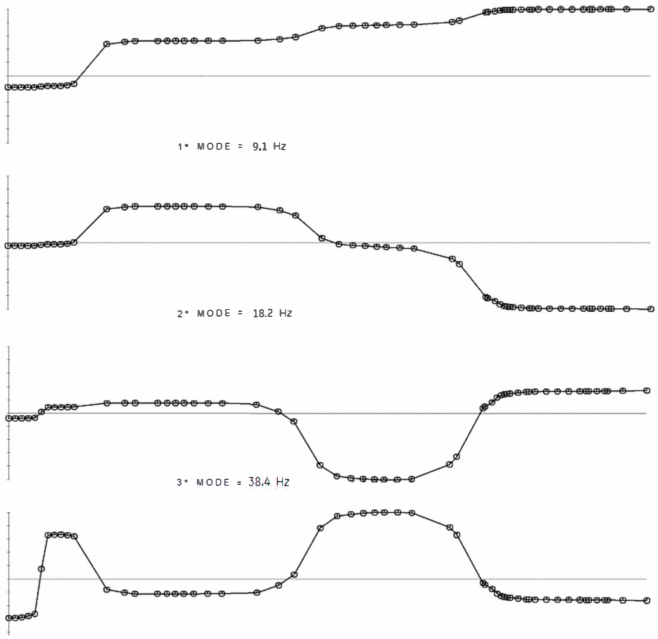

Fig. 2. Mode shapes related to the first four TNFs
Normalized amplitude vs. train section

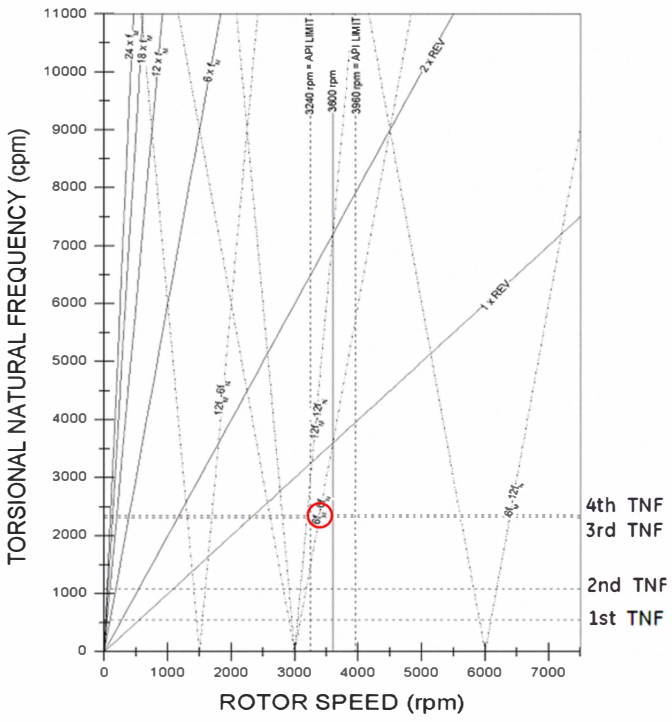

Fig. 3. Campbell diagram

The dynamic behavior of the train has been recorded by means of a dedicated data acquisition system able to record and monitor in real time both main electrical and mechanical variables, including mechanical torque (average and ripple) acting on the train shafts. In particular the following parameters have been acquired for later analysis:

- VSDS control system variables: DC-link reference and actual value, rectifier and converter firing angle, motor speed reference value
- Mechanical variables: torque on coupling C1 (measured with a strain gauge [6]) and train actual speed.

1) Modal Analysis

A lumped elements model has been adopted to calculate the train torsional response, in agreement with API 684 [5] and API 617 [10] recommendations. The train is divided in 57 rigid inertias, connected by massless torsional springs. This allows a proper description of the stiffness of each shaft section, including coupling connections and shrink fits.

Torsional natural frequencies (TNFs) of the system are calculated, performing an eigenanalysis on equations of motion (modal analysis). In the modal analysis, damping is not considered since the low structural damping does not significantly affect the value of resonant frequencies and mode shapes [9]. The equations in matrix form are:

$$[J]\ddot{\theta} + [K]\theta = 0 \qquad (1)$$

where $[J]$ is the diagonal inertia matrix and $[K]$ is the tri-diagonal stiffness matrix. The vector θ contains the degrees of freedom of the system, which are the rotations of each section around the shaft axis.

The system is underconstrained, so that there is a zero solution that is related to the rotation of the rigid body. The non-zero solutions are the TNFs. The modal shapes related to the first four TNFs are plotted in Fig. 2.

Couplings are selected to be the least stiff shaft-line components. As a consequence, the first three mode shape deformations are concentrated in the couplings, while the machine shafts are not significantly deformed. Therefore the first three TNFs are mainly a function of coupling stiffnesses and rotating machine inertias [5]. The fourth TNF involves coupling and GT shaft that is torsional less stiff due to the shaft length, with respect to the compressors and the electrical motor.

The coupling C1 is the most critical point in terms of mechanical response with respect to alternating torque developed during transient operations. Thus transients have been found to be strongly interacting with the 1st TNF. The interaction in the operating range between TNFs and possible torsional mechanical excitation are represented in the Campbell diagram [9] of Fig. 3.

Torsional excitations included in the diagram are those at

978-1-4244-9500-9/11/$26.00 © 2011 IEEE

1X revolutions (synchronous excitations due to centrifugal compressors), 2X revolutions (related to misalignments of couplings), kX motor electrical frequency (with k = 6, 12, 18 and 24, related to motor side converter harmonics and lmX grid frequency fN ± nX motor electrical frequency fMl (with m,n = 6,12, related to the convolution product of the grid side and motor side harmonics, also known as non-integer harmonics or interharmonics) ([15],[25],[26]).

API standards [5] require that TNFs of the full train shall be at least 10% above or 10% below any possible excitation frequency within the specified operating speed range, delimited by minimum operating speed (MOS) and maximum continuous speed (MCS). These limits are defined in Fig. 3 by two dashed vertical lines, labeled API LIMIT. The 6fM-6fN crosses the 3rd and 4th TNFs in this range (red circle in Fig. 3). Fatigue verifications show that torsional stresses due to this excitation are considerably lower than endurance limits of shafts and couplings.

2) Forced Response to VSDS excitation

In order to perform a forced analysis, a mechanical damping term is included by means of the damping matrix [*C*]. The vector *T* contains the VSDS excitation applied to the shaft line. The resulting equation in matrix format is therefore:

$$[J]\ddot{\theta} + [C]\dot{\theta} + [K]\theta = T \qquad (2)$$

This equation can – with an acceptable approximation – simulate the forced response of the system, not taking into account control system closed-loop effects. Therefore, the torsional analysis results are in agreement with measurements for steady state operations (rated speed). For transient operations, especially start up; the model is acceptable only if the mechanical and electrical systems are well decoupled by means of an adequate VSDS control system optimization.

B. ELECTRICAL SYSTEM DESCRIPTION

In electrification of oil & gas applications, the application of high power VSDS around 20 MW poses challenging trade offs between simpler and more reliable, well-referenced high-power CSI (current source inverter) solutions and more complex and less referenced high power VSI (voltage source inverter) solutions. CSI in high power are represented by thyristor based LCI (load commutated inverter) drives; VSI are represented by IGCT (integrated gate commutated thyristor) or IGBT (insulated gate bipolar transistor) based converter configurations controlled by adequate pulse-width modulation (PWM) schemes.

Having said this, for a helper motor rating higher than 20 MW, the LCI solution is still attractive and the main task is to reduce its inherent disadvantages (higher torque ripple and lower grid side power quality) while harvesting its inherent advantages (high reliability, proven references, simple scalability in power). A good power grid quality can be achieved by means of an adequate number of rectifier pulses (12 or 24) and installation of specific harmonic filters. On the load side, steady state torque ripple effects can be reduced by means of a proper mechanical design of the shaft line (couplings, shafts, etc.) and driver harmonic cancellation, which can reduce air gap torque (AGT) ripple down to 1% of rated torque (normally AGT ripple is 2-3% of continuous delivered torque). This is largely presented in literature for LCI ([13],[17],[18],[25]-[27]), to some extend, also for VSI based drives.

The electrical drive system used in this application is a medium voltage VSDS based on LCI technology (see Fig. 4). Two 6-pulse thyristor rectifiers supply each one DC reactor, which are combined on one motor via respective 6-pulse thyristor based inverter output bridges. Each inverter bridge is supplying an independent winding in order to cancel air-gap torque harmonics. The converter output of 2 x 3.8kV feeds a three phase synchronous motor of 20MW nominal power and 3600rpm rated speed. The turbocompressor train is started up from standstill by means of this LCI driven motor.

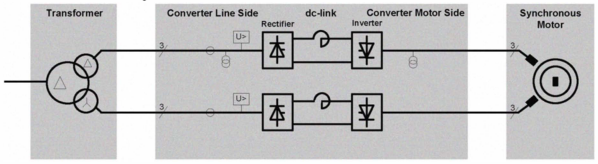

Fig. 4. Single line representation of the electrical topology of the LCI

The frequency converter controls the operation of the motor by variation of frequency and current. In order to control speed and power, it receives a torque set point from the train's speed regulator during steady operation, while during train start up it activates its own speed control loop.

The circuit and the related control theory of the LCI are well described in literature [13]. Here we only recall the relevant functions for the following measurements and analysis (Fig. 5).

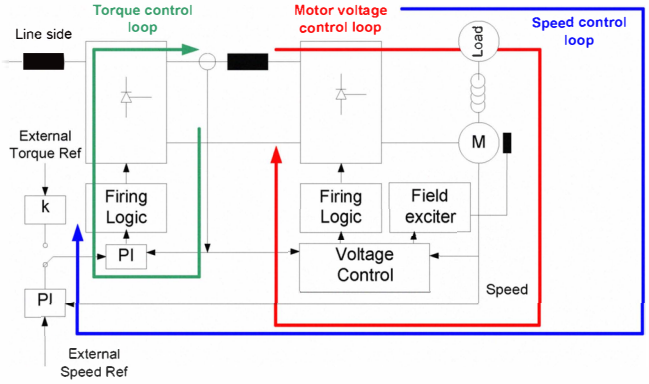

Fig. 5. Representation of LCI control system loops

The drive control platform used in the experiments measures motor voltage, i.e. the derivative of flux, and inverter currents. From these two, it calculates motor torque and motor speed. Motor voltage and torque are the controlled variables. One PI controller regulates the line rectifier bridge in order to increase or decrease DC link current and another

PI controller controls the motor voltage via the field exciter. The motor side rectifier bridge is controlled to maximum rectified voltage for the given DC current. This ensures minimal reactive power load to the network for a given load-point. From a control perspective, the current controller PI is acting in the 10ms range, the motor side rectifier firing angle needs to be adjusted in the 100ms range, and the motor voltage controller needs to act in the 1s range.

Thyristors are switched on and off to allow the current flow in the motor windings, U,V,W according to the scheme shown in Fig. 6. In one stator cycle there are 6 transitions in each converter bridge which take place every $1/6^{th}$ of the electrical fundamental period. For 2 pole machines this is identical with the motor mechanical frequency (train speed). These transitions are called commutations.

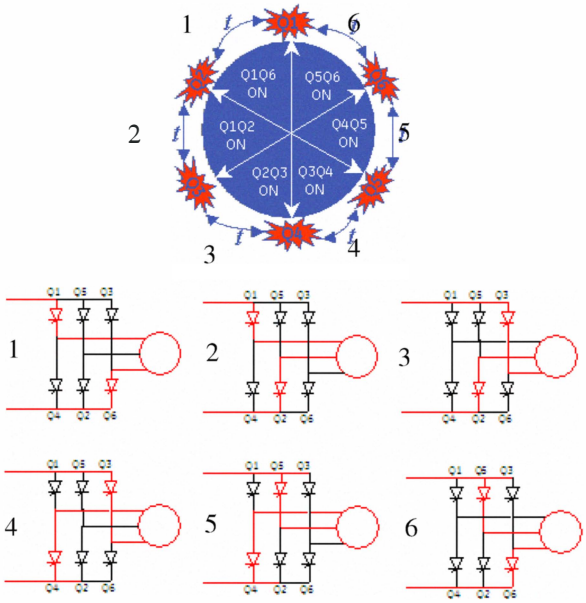

Fig. 6. Switching scheme of a thyristor based LCI

A digital control system decides on the exact timing of the commutation within the fundamental cycle. However the current will only commutate into the new position when pushed by the motor voltage. Physically, this voltage is the back EMF, generated by the load. This load commutated mode of operation also reflects in the technology name LCI.

At very low speeds, the motor cannot generate enough back EMF and the thyristors need to be forced to commutate by special control action on the line side rectifier. This operating mode is also known as pulse mode, and it lasts until 6 to 15% of rated speed, depending on the characteristics of the electric motor. For electrical design reasons, the drive in this study has a limitation in thyristor conduction time, which would in pulse mode be exceeded for very low speeds (less than 2% of rated speed). In this regime, the thyristor semiconductors are additionally turned off after a maximum conduction interval to comply with this limit.

The pulse mode and the transient between pulse and load commutated mode are the most critical conditions that need to be optimized for smooth train acceleration in order to avoid unwanted alternating torque peaks. The analysis presented in this paper highlights the main relationships that exist between closed-loop control functions, train transients and train electro-mechanical interactions. In particular experimental results obtained with different control system parameters will be presented in the next section and a detailed explanation of the train's torsional behavior will be given.

III. Experimental Results

This section reports a selection of experimental data collected during the torsional assessment of the electro-mechanical system. Train torsional performance comparison has been done verifying the effect of different inverter control setups for:

- Speed at transition from pulse mode to load commutated mode
- Helper motor speed sensor filtering
- Thyristor related maximum conduction interval
- DC current limit resp. maximum torque limit

The VSDS speed control loop is responsible to ramp the train from 0 to crank speed, typically to 10-12% speed. For the remaining part of the start up curve, the speed control is handed over to the gas turbine control system that sends a torque request to the converter control system. Requesting higher motor airgap torque (increasing the DC link current) will accelerate the train speed to achieve the gas turbine control system's speed reference. In this latter part of the start up sequence, the acceleration happens smoothly, since the converter is naturally commutated and the converter control action is slow and relatively soft, while on the other hand the first part of the starting sequence has been observed to be the most critical for the following reasons:

- Continuous torque has a lower value, so that relatively small torque peaks can lead to inverse torque, which in turn can lead to coupling fretting or gear backlash (in case of geared applications)
- At low load, the damping due to gas compression is negligible, so that the overall mechanical damping is minimal
- During the switching from pulse to load commutated mode, the VSDS control action is comparatively strong (details explained in the discussion section)

The test campaign has been carried out according to the following plan with Test #1 through Test #6:

978-1-4244-9500-9/11/$26.00 © 2011 IEEE

1) Detection of the torsional natural frequencies up to the 4th mode
2) Testing of start up with (pre-engineered) baseline parameters
3) Testing of start up modifying switchover speed for pulse mode to load commutated mode
4) Testing of start up modifying speed measurement method
5) Testing of start up modifying maximum conduction interval
6) Testing of start up modifying DC link current limit and thus maximum torque

A. *Test #1*

Test #1 has been carried out running the turbocompressor train at rated speed with GT and electric motor both in operation. Then the motor load has been suddenly removed by tripping the converter, while the GT was able to keep the speed constant (increasing exhaust temperature). The sudden motor torque shedding injects a load step-change in the system, producing a broad band torsional excitation that is able to excite the first four TNFs (Fig. 7). The step response is spectrally analyzed applying FFT to the time-domain signal over the entire torsional oscillation decay. This yields the spectrum shown in Fig. 8.

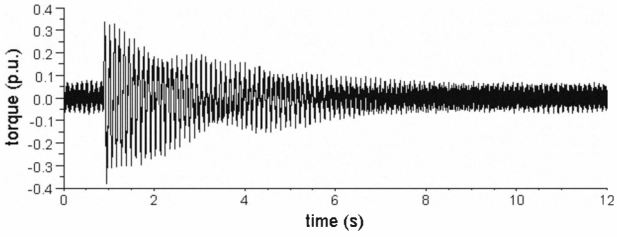

Fig. 7. Alternating torque after helper motor load shedding (test #1)

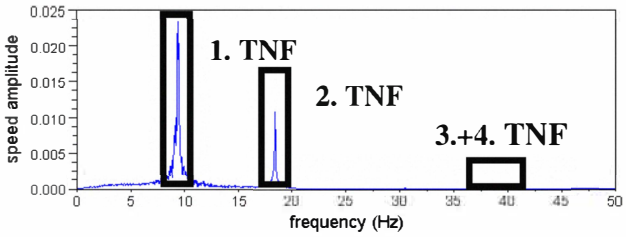

Fig. 8. Spectrum of alternating torque after load shedding

Test results show that the torsional excitation involves mainly the 1st and 2nd TNF, while the 3rd and 4th TNF are marginally excited. Higher modes can be neglected, since they do not participate to the torsional oscillation phenomena. The frequencies of the first four torsional modes are presented in the following table:

TABLE I
FREQUENCIES OF PREDOMINANT MODES

TNF (Mode)	Frequency [Hz]
1st	9.5
2nd	18.5
3rd	38.3
4th	39.5

B. *Test #2*

Before running the start up with baseline parameters, the measured TNFs have been plotted in a Campbell diagram, focusing on the start up speed range, in order to highlight the most critical torsional resonances (co-incidence of excitation and TNF) of the VSDS' integer exciting torques with the first two dominant torsional modes (see Fig. 9).

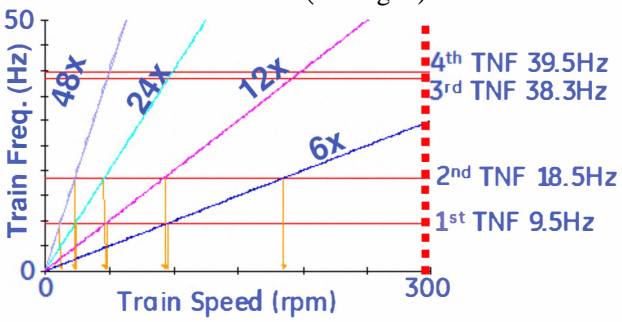

Fig. 9. Detail of Campbell diagram

The dotted vertical line is the switchover speed from pulse mode to load commutated mode in baseline configuration. The first start up was run with the following configuration:

- Switchover speed = 8.5% of rated speed
- VSDS speed measurement = with encoder
- Maximum thyristor conduction interval = 210 ms
- DC current limit = 25% of nominal torque

During start up, the converter has been set up to operate at the DC-link current limit. This means maximum producible torque, in order to ride through the transients as quick as possible. This is widely considered best practice in the industry.

The alternating torque measurement in Fig. 10 shows the presence of two peaks: the first is developed around 47rpm (20% of rated torque, 0-pk), the second around 355rpm (25% of rated torque, 0-pk). The measurement highlights a different decay of the alternating torque peaks, which suggest that the two phenomena have different root causes and dynamics.

The analysis of the waterfall plot in Fig. 11 shows the direct excitation of the train TNFs by the VSDS integer harmonics during pulse mode operation, with a predominant excitation of the 1st TNF and a lower excitation of the 2nd TNF – both by the 24th harmonic of the VSDS pulsating torque – and a mild excitation of the 3rd and 4th TNFs. The second peak, which is developed at pulse to load commutated mode switchover, involves the 1st TNF only, but it is not related to any VSDS integer excitation.

978-1-4244-9500-9/11/$26.00 © 2011 IEEE

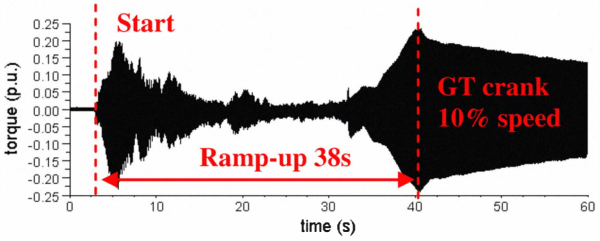

Fig. 10. Alternating torque measured during start up in test #2

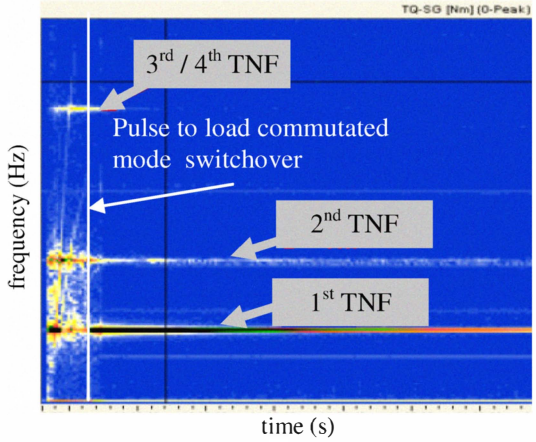

Fig. 11. Waterfall plot of the alternating torque (test #2)

C. *Test #3*

In the test run #3, the speed at which the control switches from pulse to load commutated mode has been changed from 8.5% to 6% of rated speed. The corresponding alternating torque measurement is shown in Fig. 12. The second peak, at 355rpm, has disappeared; while the peak at low speed (47rpm) is still present (28% of rated torque).

In the corresponding waterfall plot Fig. 13, one is able to identify the strong excitation of the 1st TNF by the 24th of the VSDS pulsating torque, a relatively small excitation of the 2nd TNF (mainly by 12th and 24th) and the mild excitation of the 3rd TNF by the 24th, all during pulse mode; but there is no additional excitation of the 1st TNF during the start up sequence.

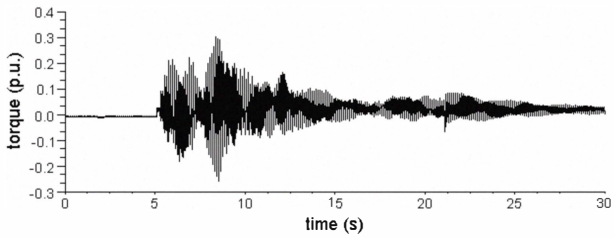

Fig. 12. Alternating torque measured during start up in test #3

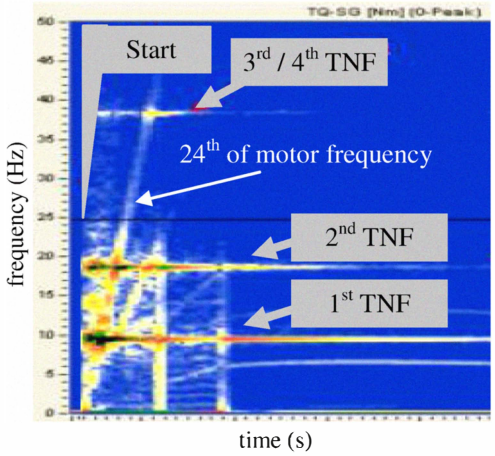

Fig. 13. Waterfall plot of the alternating torque (test #3)

D. *Test #4*

In the 4th run, the switchover from pulse to load commutated mode has been restored to the baseline value (at 8.5% of rated speed) and the speed measurement system has been switched from encoder to observer. The observer estimates the speed from the machine flux vector, which is calculated from the motor stator voltage. The flux vector's derivative corresponds to nx*flux-amplitude. Dividing the derivative by the flux vector amplitude will yield the electric stator frequency ω_X. Finally, the stator frequency can be used to calculate the speed in rpm, since

$$f_{Mech}[Hz] = f_{elect}[Hz] \cdot p = \frac{\omega_X}{2\pi} \cdot p \qquad (3)$$

with [p] being the number poles pairs and

$$RPM = f_{Mech}[Hz] \cdot 60 \qquad (4)$$

The alternating torque measurement is shown in Fig. 14. The events at low speed are still present (25% of rated torque, 0-pk), on the other hand the second peak at 355rpm is not present, contrary to the first start up attempt carried out using encoder speed measurement.

The waterfall analysis in Fig. 15 confirms that the only alternating torque peaks present during start up #4 are the ones caused by the direct excitation of the TNFs by converter integer harmonics, mainly the 12th and 24th.

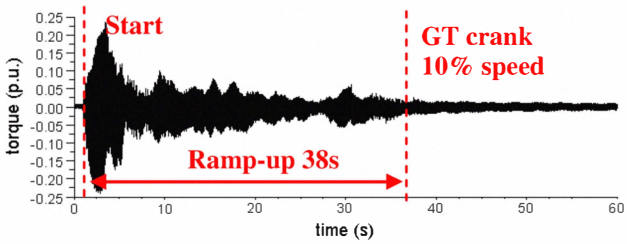

Fig. 14. Alternating Torque Measured during start up in test #4

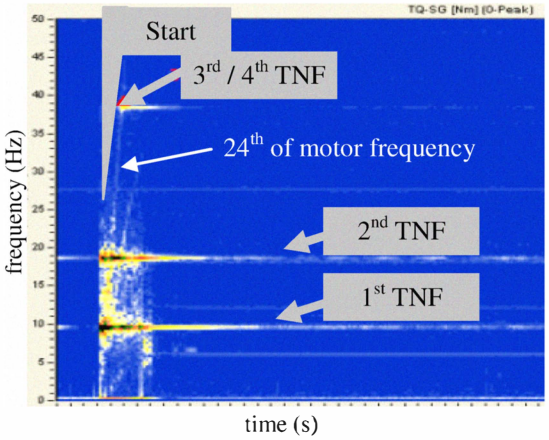

Fig. 15. Waterfall of the alternating torque (test #4)

E. *Test #5*

Test #5 has been carried out using observer-based speed and modifying the maximum conduction interval of one thyristor branch from 210ms to 150ms. The other parameters have been left unchanged with respect to the baseline configuration.

The alternating torque measurement is shown in Fig. 16. The peak at low speed is drastically reduced (6% of rated torque; 0-pk), and the peak at 355rpm is confirmed to remain cancelled.

The waterfall plot Fig. 17 confirms that the first two TNFs are less excited by the 12th and the 24th integer harmonic of the VSDS. The response of the 3rd and 4th TNFs is not changed and it is still at a low level.

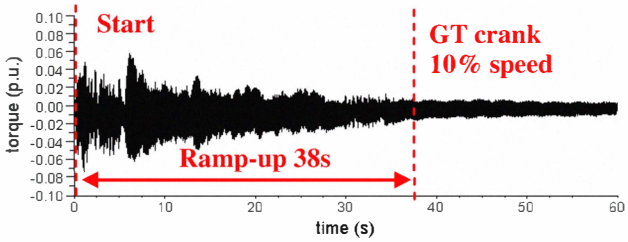

Fig. 16. Alternating torque measured during start up in test #5

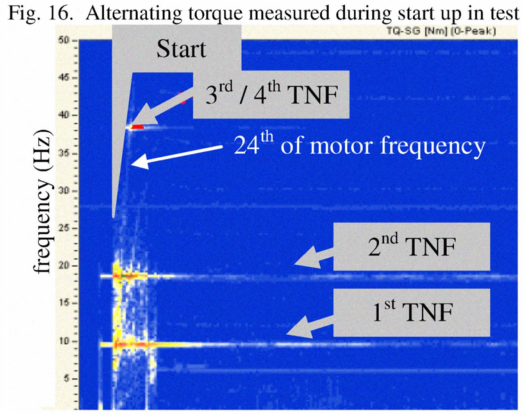

Fig. 17. Waterfall of the alternating torque (test #5)

F. *Test #6*

A last test has been carried out with the same configuration as in test #5, but reducing the DC-link current limit, and thus the accelerating torque maximum, from 25% to 12.5% of nominal torque.

The results are shown in Fig. 18 and 19. The torque peak is nearly halved (4% of rated torque; 0-pk) due to the reduction of air-gap torque. Of course this reduction doubles the time to ramp up from 0 to crank speed.

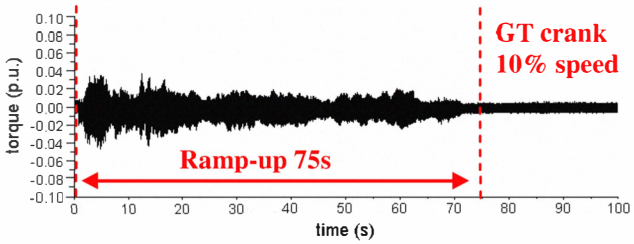

Fig. 18. Alternating torque measured during start up in test #6

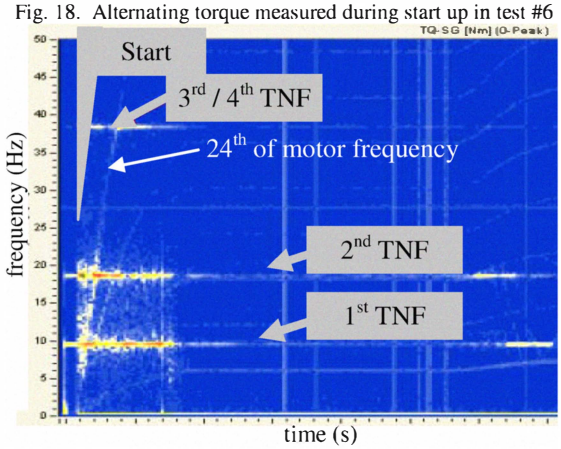

Fig. 19. Waterfall of the alternating torque (test #6)

A detailed explanation of the electro'mechanical behavior experienced during the test campaign is presented in the discussion session, especially with reference to the torque peaks recorded, in some specific configurations, at 47rpm and 355rpm.

IV. DISCUSSION

The two main torsional interaction phenomena encountered during the test campaign are the torque peak in test #2 at 355rpm and the torque peak in tests #2, 3 and 4 at 47rpm. Their causes have been found to be fundamentally different.

A. *Torque peak event at 355rpm*

To investigate the origin of the high alternating torque event at 355rpm, a detailed analysis of VSDS control parameters has been carried out. In particular the following dynamic variables have been analyzed:

- Speed encoder signal
- Current reference signal
- DC link current signal
- Motor side thyristor firing angle signal

They are indicated in a simplified VSDS control system block diagram in Fig. 20. The speed encoder signal is represented with blue color, the current reference signal with red color, the DC-link actual current signal with green color and the motor side thyristor firing angle signal with orange color.

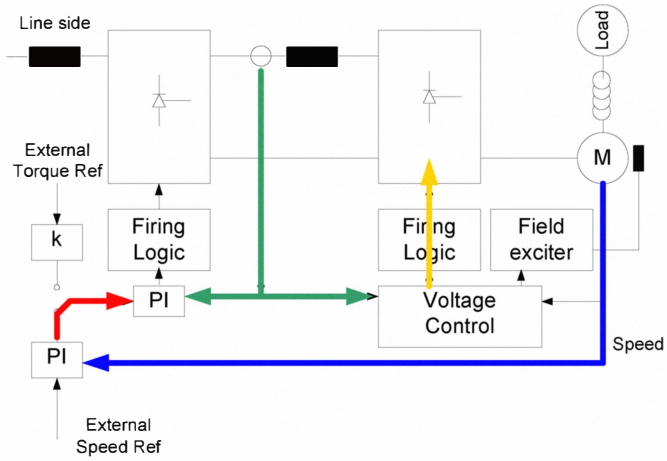

Fig. 20. VSDS key control signal location in control system block diagram

The dynamic signal of the encoder recorded during the 355rpm torque event is shown in Fig. 21. The presence of an oscillating part which increases once the torsional event is established is evident. The spectral analysis reveals a significant component at the frequency of the 1st TNF (see Fig. 21).

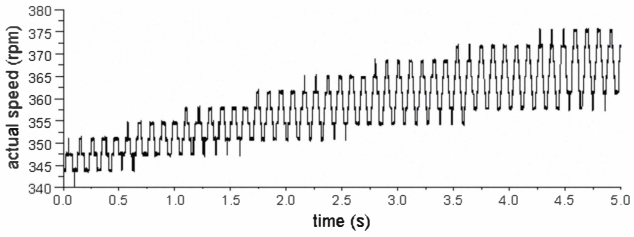

Fig. 21. Encoder signal at the 355rpm torque peak

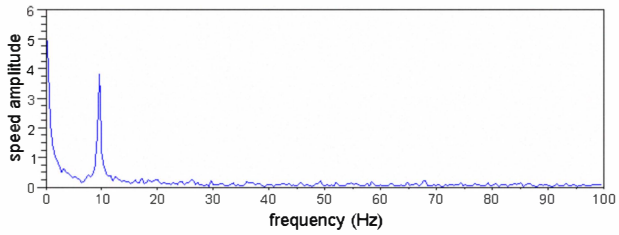

Fig. 22. Spectrum of encoder signal during 335rpm torque peak

In the speed control loop, the speed signal is matched against the reference speed ramp, and the error generates the current reference signal. The speed controller, having enough bandwidth, responds to the measured speed oscillations, and is producing a pulsation at 9.5Hz in the current reference signal as well (Fig. 23 and 24).

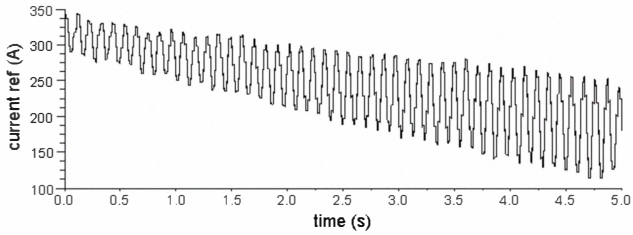

Fig. 23. Current reference signal at 355rpm torque peak

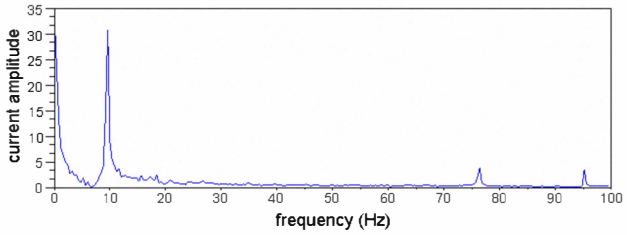

Fig. 24. Current reference signal spectrum during 355rpm torque peak

The pulsating current reference is compared to the actual DC-link current value. This error produces – as part of the current controller – the net side thyristor firing angle command, which closes the DC-link current feedback. The 9.5Hz pulsation is then established in the DC-link current (Fig. 25 and 26)

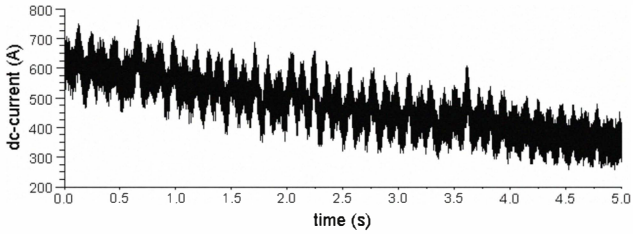

Fig. 25. DC-Link current signal at 355rpm torque peak

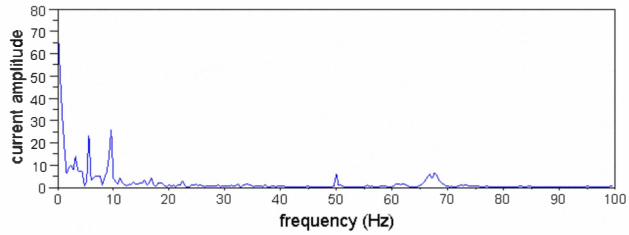

Fig. 26. DC-Link current signal spectrum during 355rpm torque peak

Other components in the spectrum are the 1st, the very small 6th, the grid frequency (50Hz) and the 12th, which are not involved in the alternating torque peak event.

Furthermore, the current actual value is used by the VSDS

controller to determine the reference function for the motor side thyristor firing angle, in order to set the VSDS power factor. Due to the pulsating component in the DC-link current signal, the motor firing angle contains a dynamic part around 9.5Hz as well (Fig. 27 and 28), and as a final result another excitation at 9.5Hz is generated.

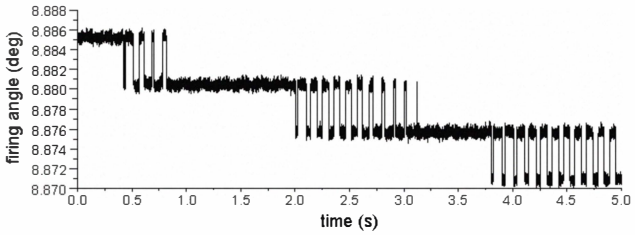

Fig. 27. Thyristor firing angle on motor side at 355rpm torque peak

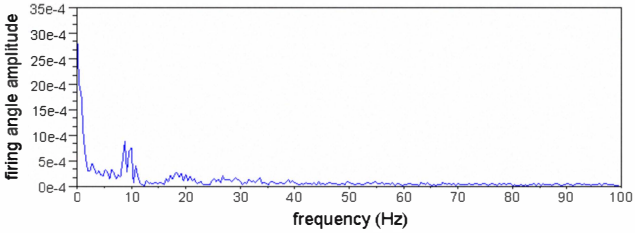

Fig. 28. Thyristor firing angle spectrum during 355rpm torque peak

The torsional interaction is initiated during switchover from pulse mode to load commutated mode, where a broadband noise is generated in the control loops. In Fig. 29a (left) and 29b (right) the current reference signal is shown immediately before and after the switchover, both in time- (above) and in frequency-domain (below).

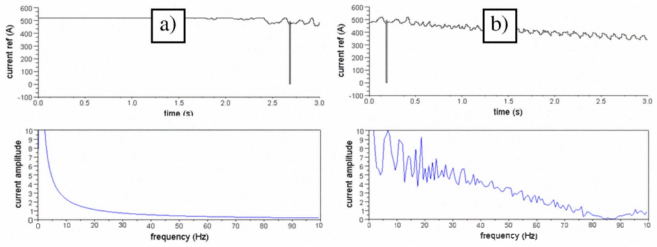

Fig. 29. Current reference (top) and its spectrum (bottom) during switchover from pulse mode to load commutated mode: a) shortly before, b) after

After control loop transients have settled, a small dynamic component at the 1st TNF remains (Fig. 30). Such pulsations, once established, create a self sustaining limit cycle according to the mechanism previously described.

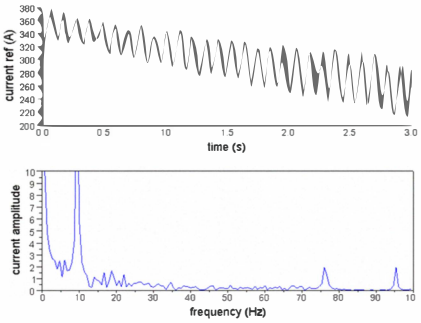

Fig. 30. Current reference after settling of transients

0-Pk dynamic torque has initially a relatively low magnitude (around 2.5%) but it initiates the control system reaction around 1st TNF in Fig. 31. The entire torque peak development takes around 8 seconds (Fig. 32). This behavior is fundamentally different from a pure mechanical resonance, where the response develops itself in shorter time, depending on the mechanical characteristics.

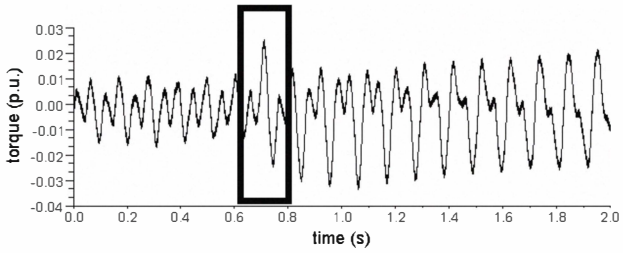

Fig. 31. Mechanical torque response during switchover

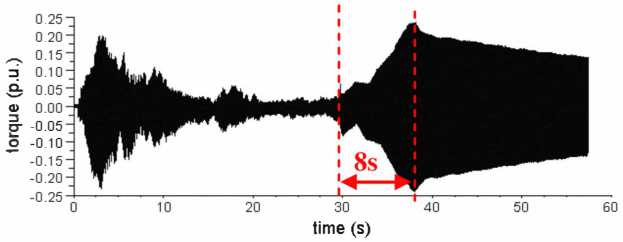

Fig. 32. Development of the self-sustaining limit cycle in the mechanical torque response

During pulse mode the speed controller operates in a feed forward mode and the feedback loops are left open. In other words, the VSDS develops torque according the DC-link limit irrespective of the motor mass behavior. At the switchover to load commutated mode, the feedback loops are closed and the reference ramp initialized to calculate the speed error to be corrected (Fig. 33).

978-1-4244-9500-9/11/$26.00 © 2011 IEEE

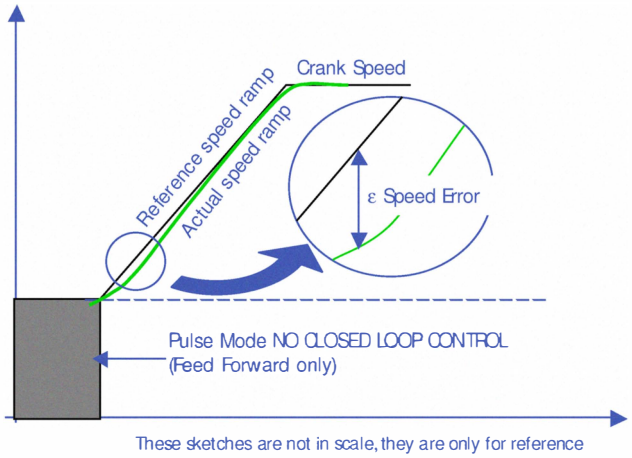

Fig. 33. Sketch of the reference speed ramp vs. actual speed

The speed error (ε) and the speed controller parameters (kp and Ti) are the main factors that determine the system dynamic behavior. The speed error is a function of the speed reference ramp and the system actual speed; the larger the error the stronger is the control action. Consequently, small signal thinking, assuming linear behavior, is not feasible anymore.

A key point is the switchover from pulse mode to load commutated mode, when the speed control loop is activated. Depending on the speed error and the DC link current value (actual and reference) there can be completely different interactions (see Fig. 34). It has to be noted that the reference ramp is initialized each start up, since the time when the train will reach switchover speed is initially not known and can vary in each start up due to different load configurations.

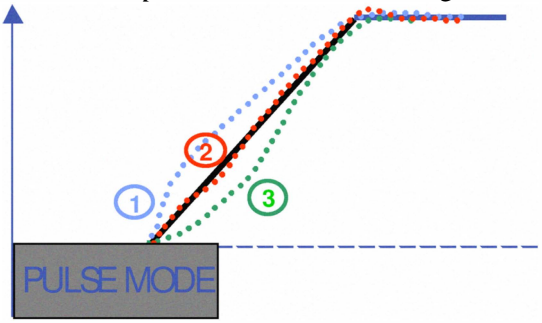

Fig. 34. Different start up dynamic depending by initial conditions at pulse to load switchover

1. Negative error: Initialized control parameters (mainly current reference) are too high with respect to the reference ramp. Strong control action to reduce the current.
2. Negligible error: Initialized control parameters are according to speed reference ramp. Control system follows the reference smoothly.
3. Positive error: Initialized control parameters are too low. Strong control action to increase current.

During test #3, by modifying the switchover speed, the controller has changed from start up curve shape 1 to curve shape 2 (see Fig. 35 and 36)

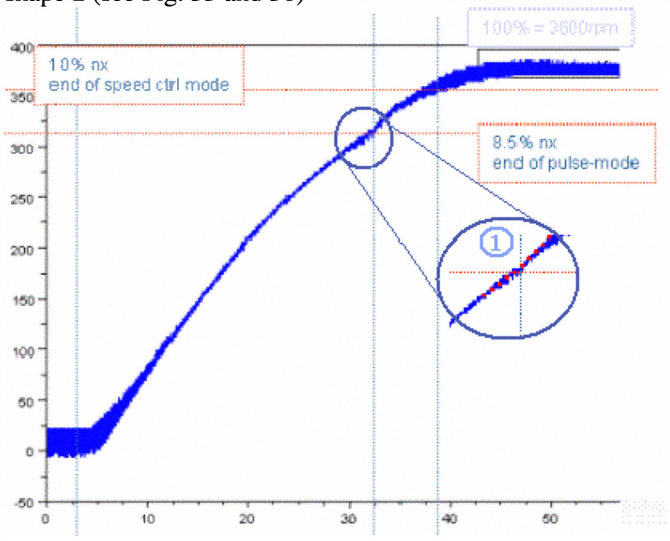

Fig. 35. Start up curve with details of the switchover speed error for run # 2

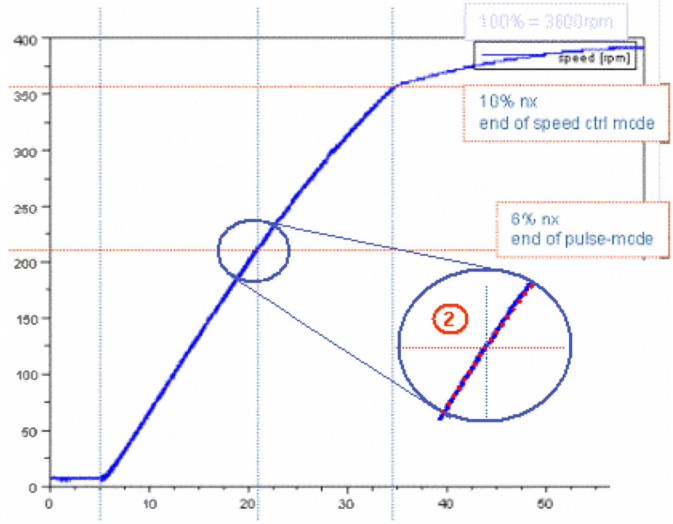

Fig. 36. Start up curve with details of the switchover speed error for run # 3

The effect on the controlled variables current and speed is the absence of a strong controller modulation at 1st TNF (9.5Hz) as shown in Fig. 37a (during switchover) and 37b (after transient settling), which should be compared to Fig. 29b with its strong modulation in the frequency domain.

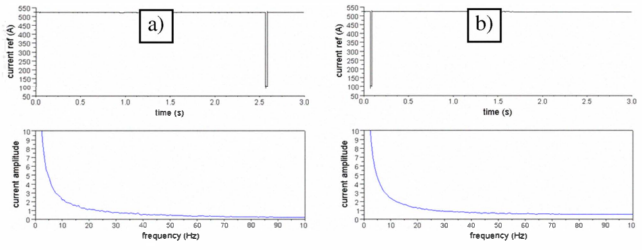

Fig. 37. Current reference (top) and its spectrum (bottom) at switchover from pulse mode to load commutated mode for test # 3:
a) before, b) after transient settling

To be more specific, in test #2, after pulse mode to load commutated mode switchover, the current reference value is strongly reduced:

- Current reference at switchover = 510A
- Current reference at switchover + 1sec = 400 A

The strong modulation of the current continues up to crank speed with the presence of a 9.5 Hz component (see Fig. 29a, 29b and 30).

In test #3 however, the current reference is almost unchanged. The current reference modulation takes place smoothly

- Current reference at switchover = 523 A
- Current reference at switchover + 1 sec = 522 A

All over the ramp up to crank speed there is no closed loop interaction at 9.5 Hz (see Fig. 37a and b).

B. General law for a self sustaining torsional limit cycle

A general law for a self sustaining torsional limit cycle can be proposed:

- The pulsation in the VFD control loop at TNF is a sufficient condition.
- The strong modulation of the control loop is a necessary condition.

The general law is in agreement with the results of test #4, where the speed measurement is switched from encoder to observer. A comparison of the actual speed signal as seen by the VSDS and of the current reference signal, measured during test run #2 and test run #4, is presented in Fig. 38 and 39 as spectra. The component in the control loop signal at the 1st TNF is no longer present, since the observer introduces a low pass filtering in the speed control loop that prevents the establishment of the self sustaining limit cycle.

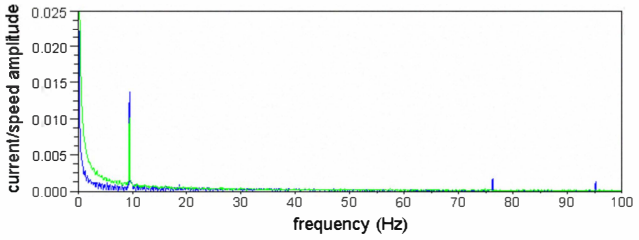

Fig. 38. Current reference and speed signal spectrum during start up test # 2

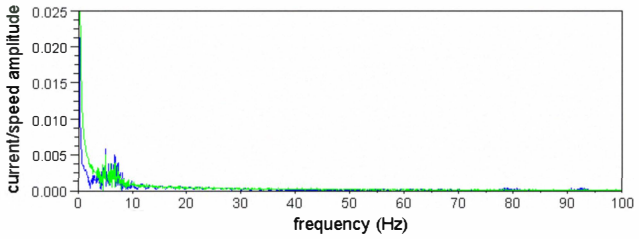

Fig. 39. Current reference and speed signal spectrum during start up test #4

The establishment of the limit cycle introduces a negative damping in the system. This is due to the interaction between controller and mechanical system, which ultimately increases the torsional sensitivity of the train, even outside of direct excitation of any mechanical resonance.

The inherent electrical damping is:

$$D_e = \frac{\partial}{\partial \omega} T_e \tag{5}$$

The torque can be expressed as:

$$T_e(t) = \frac{P_e}{\omega(t)} \tag{6}$$

Hence

$$D_e = \frac{\partial}{\partial \omega}\frac{P}{\omega(t)} = \frac{1}{\omega(t)}\frac{\partial P}{\partial \omega} + P\frac{\partial}{\partial \omega}\frac{1}{\omega(t)} \tag{7}$$

Which gives:

$$D_e = \frac{1}{\omega(t)}\frac{\partial P}{\partial \omega} - \frac{P}{\omega(t)^2} \tag{8}$$

The second term of the expression is always negative; the first term is negative when the differential of power and speed are opposite-sign and positive when they are like-sign.

Normally the controller reacts in such a way that if the speed increases the power is reduced, and vice versa, implying a negative first term as well. The solution to overcome this is to avoid controller reaction at TNFs, where the responses are magnified, or to prevent strong controller modulation, for instance with soft PI settings and by avoiding saturation of control loops.

C. Torque peak event at 47rpm

A zoom of the low speed range of the start up sequence evidences the excitation by integer harmonic components of the pulsating torque (6xfM, 12xfM, 24xfM and 48xfM, with fM = actual motor stator frequency).

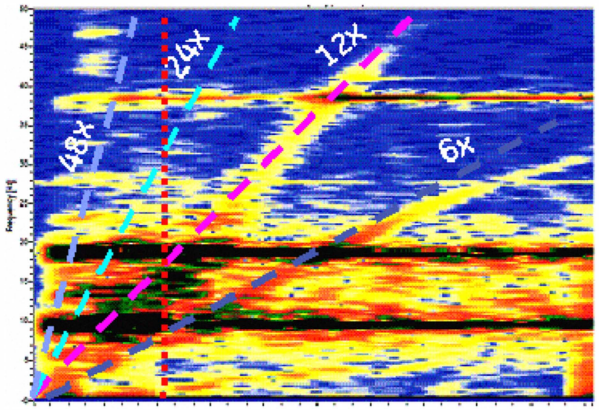

Fig. 40. Coupling torque waterfall in low speed range of train start up

In particular, an unexpected magnitude of peak torque is present in the resonance condition of the 12xfM over the 1st TNF, which takes place at 47.5rpm (12x fM = 570cpm, fm= 570/12=47.5cpm). Higher torque response is due to the presence of a supplementary excitation source related to the additional turn off of thyristors in the speed range 0-2%. As explained in the system description section, in one stator cycle there are 6 semiconductor transitions in each converter bridge. They take place every 1/6th of the electrical fundamental period that for 2 pole machines coincides with the motor mechanical frequency (train speed). In the low speed range the thyristor conduction time is longer. By electrical design, the maximum conduction time is limited to 210ms. The critical speed is

$$n_{limit} = \frac{10}{t_{charging} \cdot polepair} = \frac{10}{0.210 \cdot 1} = 47.62\text{rpm} \quad (9)$$

Below this speed, additional commutations are required. These commutations shall take place at least each 210ms, regardless of output frequency, and it impacts the alternating torque spectra. Fig. 41 shows the DC-link current in the low speed range, additional commutations (spaced by 210ms) are highlighted in yellow boxes. Normal forced commutations, not spaced by 210ms, are highlighted in blue boxes.

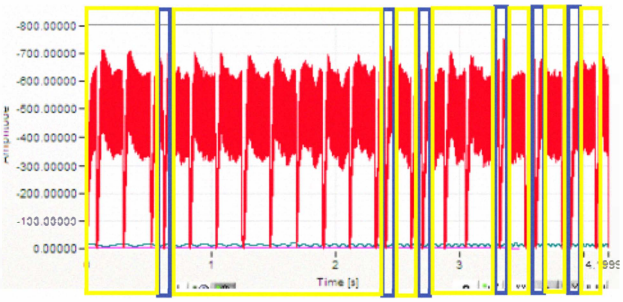

Fig. 41. DC-Link current during start up in the low speed range

The traditional best practice for such extra commutations is to wait for the maximum interval, as this would give the minimum number of extra torque pulses. However for torsional resonance phenomena, time-domain is not revealing the full truth. But it is possible to determine the effect in frequency domain, considering and not considering the additional commutations. Above 47rpm (0.783Hz) there is no influence, below 47rpm 12xfM and 24xfM harmonics presents local maxima and minima, and in particular there is a local maximum around 47rpm, in agreement to the measurement done (see Fig. 42).

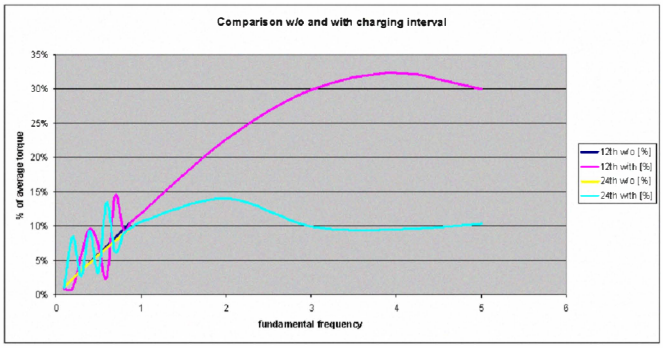

Fig. 42. Comparison of airgap torque pulsation harmonics amplitude with and without extra commutations

Knowing this, it is possible to change the maximum conduction interval in order to optimize the torque response in the low speed range. Such a modification can be done only by reducing the interval, since the time elapsed between two forced commutations cannot be more than 210ms.

An analysis has been done to verify the impact on harmonic content reducing the maximum conduction interval, and it has been observed that the level of excitation can be reduced by selecting the interval so that, in correspondence to TNF crossing frequencies, the components of excitation have local minima. To better understand this concept, a map has been implemented (Fig. 43). Black color identifies areas with at least one harmonic component higher than with no extra commutations; white color identifies areas having ALL the harmonic components lower than without extra commutations, while the grey marked area is not affected by the maximum conduction interval selection.

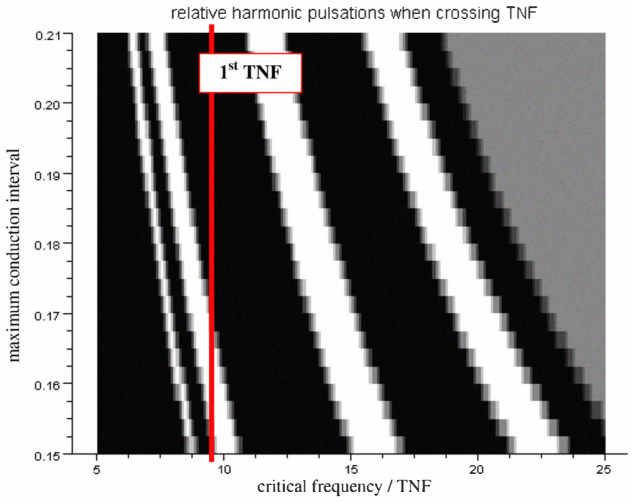

Fig. 43. Sensitivity analysis on charging time impact on pulsating torque harmonic components.

The study shows that 150ms is the best maximum conduction interval with respect to the train's TNFs. This result has been validated by the test campaign, which confirms the cancellation of the torque peak at 47rpm, visible by comparing Fig. 14 (test #4 with 210ms) to Fig. 16 (test #5 with 150ms).

978-1-4244-9500-9/11/$26.00 © 2011 IEEE

V. CONCLUSIONS

Integration of VSDS in oil and gas trains poses significant challenges, which are not limited to the normal operating conditions, but, conversely, are even more significant during transient conditions, such as train start up and acceleration.

By applying a rigorous train system integration approach, which considers electromechanical coupled effects, controller dynamics and detailed shaft line modeling and analysis, it is possible to implement all the necessary solutions in order to overcome any adverse effect due to the electromechanical interaction between VSDS and mechanical system.

In particular, it is possible to select parameters to optimize system response during transient conditions. The configuration can be validated by means of dedicated tests that can be carried out during a turbocompressor string test (FAT, factory acceptance test) and/or directly at site during commissioning or even later during operating life.

VSDS application in oil and gas trains (LNG-helper or motor-compressor configurations) is not free of concerns, but expertise of the electrical and the mechanical system manufacturer in system integration can reduce potential torsional issues and can be a significant guidance in adopting the best trade off (reliability vs. performance) for each specific application among the existing VSDS technologies.

REFERENCES

[1] R. Baccani, R. Zhang, T. Toma, A. Iuretig, M. Perna, "Electric systems for high power compressor trains in oil and gas applications – system design, validation approach and performance", Proc. of 36th Annual Turbomachinery Symposium.

[2] M.A. Miranda, E.S. Brick, "Life Cycle Cost Assessment of Turbomachinery for offshore applications", Proc. of 33rd Annual Turbomachinery Symposium.

[3] A. Kocur, Jr., J.P. Corcoran, "VFD Induced Coupling Failure", Case study of the 37th Annual Turbomachinery Symposium

[4] T. Shimakawa, T. Kojo, "The Torsional Torque Fluctuations of Compressor Train with Vector Control PWM Inverter", Case study of the 36th Annual Turbomachinery Symposium

[5] API 684 Rotordynamic Tutorial: *Lateral Critical Speeds, Unbalance Response, Stability, Train Torsionals and Rotor Balancing*

[6] H.N. Norton, *Sensor and Analyzer Handbook*, Prentice Hall, 1982.

[7] S.S. Gindy, *Force and Torque Measurements, A Technology Overview Part Two – Torque*, Wiley InterScience, Experimental Techniques, Volume 9, Issue 7

[8] D. Lambrecht, T. Kulig, "Torsional Performance of Turbine-Generator Shafts especially under resonant excitation", *IEEE Transactions on Power Apparatus and Systems*, vol. PAS-101, No. 10 October 1982

[9] D. Walker, *Torsional Vibration of Turbo-Machinery*, USA, Mc Graw-Hill, 2003

[10] API 617 Axial and Centrifugal Compressors and Expander-compressors for Petroleum, Chemical and Gas Industry Services

[11] P.L. Gatti, V. Ferrari, *Applied Structural and Mechanical Vibrations*, Taylor and Francis, 2003

[12] B.T. Ooi, "Phase Modulation Theory of electromechanical damping in synchronous generator", *IEEE Transactions on Power Apparatus and Systems*, vol. PAS-100, No. 5, May 1981

[13] A. Kloss, *A Basic Guide to Power Electronics*, John Wiley & Sons, 1984

[14] D.N. Walker, S. L. Adams, R. J. Placek, "Torsional Vibration and Fatigue of Turbine-Generator Shafts", *IEEE Transactions on Power Apparatus and Systems*, vol. PAS-IOO, No. 11 November 1981

[15] Peterson R.E. *Stress Concentration Factors (2nd edition)*, John Wiley & Sons, 1997

[16] J.E. Shigley, *Mechanical Engineering Design*, ASME Transactions, Mc-Graw Hill Series in Mechanical Engineering

[17] A. Kloss, R. Lubasch, K. Schweizer, "Interaction between large converter-fed variable-speed AC drives and power supply systems", CIGRE 1992 Session, Paris.

[18] A. Kloss, *Netzrückwirkungen der Leistungselektronik*, VDE Verlag, 1996.

[19] J.C. Wachel, F.R. Szenasi, "Analysis of Torsional Vibrations in Rotating Machinery", Proceedings of the 22nd Turbomachinery Symposium

[20] G. Genta, *Vibration of Structures and Machines - Practical Aspects*, Second Edition, Springer-Verlag

[21] R. B. Randall, *Frequency Analysis (3rd edition)*, Bruel & Kjaer, Naerum, Denmark.

[22] C. Sihler, S. Schramm, J. Song-Manguelle, P. Rotondo, S. Del Puglia and E. Larsen "Torsional Mode Damping for Electrical Driven Gas Compression Trains in Extended Variable Speed Operations", Proceedings of the 38th Turbomachinery Symposium

[23] A. Lenzi, P. Jörg, S. Falomi, D. Andreo, S. De Franciscis, P. Rotondo, D. Fioravanti and T. Hattenbach, "Combined Torsional and Electromechanical Analysis of an LNG Compression Train with Variable Speed Drive System", Proceedings of the 38th Turbomachinery Symposium

[24] S. Del Puglia, S. De Franciscis, S. Van de moortel, P. Jörg, T. Hattenbach, D. Sgrò, L. Antonelli, S. Falomi, "Torsional Interaction Optimization in a LNG Train With a Load Commutated Inverter", Proceedings of the 8th IFToMM International Conference on Rotordynamics 2010, Seoul, Korea

[25] L. Terens, A. Grgic, "Applying Variable Speed Drives with Static Frequency Converters to Turbomachinery", Proceedings of the 25th Annual Turbomachinery Symposium, 1996.

[26] A. Grgic, W. Heil, H. Prenner, "Large Converter-Fed Adjustable Speed AC-Drives for Turbomachinery", Proceedings of the 21st Annual Turbomachinery Symposium, 1992

[27] J.-J. Simond, A. Sapin, M. Tu Xuan, R. Wetter, W. Ziller, "12-p LCI Synchronous Drive for a 20MW Compressor Modeling, Simulation and Measurements", Fourtieth IEEE IAS Annual Meeting. Conference 2005

[28] V. Hutten, R. Zurowski, M. Hilscher, "Torsional Interharmonic Interaction Study of 75 MW Direct-Driven VSDS Motor Compressor Trains for LNG Duty", Proceedings of the 37th Turbomachinery Symposium

978-1-4244-9500-9/11/$26.00 © 2011 IEEE